Research Square

Preprints are preliminary reports that have not undergone peer review.
They should not be considered conclusive, used to inform clinical practice,
or referenced by the media as validated information.

Ambient black carbon and its dependence on in-situ stubble burning

Vikas Goel
Indian Institute of Technology Delhi
Ajit Kumar
Indian Institute of Technology Delhi
Anjanay Pandey
Indian Institute of Technology Delhi
Mohd Faisal
Indian Institute of Technology Delhi
Umer Ali
Indian Institute of Technology Delhi
Rakesh Maity
Indian Institute of Technology Delhi
Ravindra Khaiwal
Post Graduate Institute of Medical Education and Research
Suman Mor
Punjab University
Vikram Singh
Indian Institute of Technology Delhi
Mayank Kumar
kmayank@mech.iitd.ac.in

Indian Institute of Technology Delhi

Research Article

Keywords: Crop residue burning, Black carbon, Optical properties, Punjab, Air pollution

Posted Date: February 26th, 2026

DOI: https://doi.org/10.21203/rs.3.rs-8494965/v1

License: This work is licensed under a Creative Commons Attribution 4.0 International License.
Read Full License

Additional Declarations:
No competing interests reported.

Table 1 is available in the Supplementary Files section.

Version of Record: A version of this preprint was published at Environmental Monitoring and Assessment on July 13th, 2026. See the published version at https://doi.org/10.1007/s10661-026-15679-2.

Ambient black carbon and its dependence on in-situ stubble burning

Vikas Goel[a,b,1], Ajit Kumar[a,1], Anjanay Pandey[b], Mohd Faisal[b,d], Umer Ali[b], Rakesh Maity[a], Ravindra Khaiwal[e], Suman Mor[f], Vikram Singh[b*], Mayank Kumar[a*]

[a]Department of Mechanical Engineering, Indian Institute of Technology Delhi, New Delhi, 110016, India

[b]Department of Civil and Environmental Engineering, Virginia Tech, Blacksburg, 24060, USA.

[c]Department of Chemical Engineering, Indian Institute of Technology Delhi, New Delhi, 110016, India

[d]Laboratory of Atmospheric Chemistry, Paul Scherrer Institute, Villegen, Aargau, 5232, Switzerland

[e]Department of Community Medicine and School of Public Health, PGIMER, Chandigarh 160012, India

[f]Department of Environment Studies, Panjab University, Chandigarh 160014, India

[1]Vikas Goel and Ajit Kumar contributed equally as joint first authors.

*Corresponding authors.

E-mail addresses: kmayank@mech.iitd.ac.in (M. Kumar); vs225@chemical.iitd.ac.in (V. Singh)

Authors' email addresses:

1. Vikas Goel: vikasgoel1002@gmail.com
2. Ajit Kumar: mez208088@mech.iitd.ac.in
3. Anjanay Pandey: Anjanay.Pandey@checmical.iitd.ac.in
4. Mohd Faisal: mohd.faisal@psi.ch
5. Umer Ali: UmerAli@chemical.iitd.ac.in
6. Rakesh Maity: mez218495@mech.iitd.ac.in
7. Ravindra Khaiwal: khaiwal.ravindra@pgimer.edu.in
8. Suman Mor: Sumanmor@pu.ac.in
9. Vikram Singh: vs225@cornell.edu
10. Mayank Kumar: kmayank@mech.iitd.ac.in

Abstract

Crop residue burning (CRB) in Northern India is a serious concern that poses substantial health risks and deteriorates air quality in the Indo-Gangetic Plain (IGP) region via regional transport. Despite governmental regulations and various interventions, the practice remains prevalent. In this study, we investigate the influence of CRB on ambient black carbon (BC) level in rural areas of Punjab during the post monsoon period. BC source contributors were quantified using aethalometer model (AM) and positive matrix factorization (PMF) approaches. Interestingly, despite the distinct mathematical framework of these two models, their results showed good agreement. Although, the measurements were conducted in the agricultural field, CRB contributed on average 48% to the total BC, periodically exceeding 90% during the active burning hours (1:00 PM – 6:00 PM), resulting in strong diurnal variation. In addition to the CRB several other BC sources e.g., traffic emissions (20.2%), power plant emissions (24.0%), waste incineration (2.0%), and a Pb-rich industrial factor (6.1%) were also quantified. The BC concentration measured during the study ranged from 1.45 to 85.0 μg/m³ with an average of 12.6 μg/m³. Absorption Angstrom Exponent (AAE), an important aerosol parameter, is also calculated and observed to be 1.7 ± 0.3, with hourly variations ranging from 1.1 to 2.4, suggesting a significant influence of CRB. Furthermore, spectral variation in absorption characteristics of BC and brown carbon (BrC) was also calculated, providing insight into the optical properties of fresh biomass-burning carbonaceous aerosols. These findings highlight the persistent dominance of CRB emissions in shaping rural aerosol composition. Moreover, when transported by prevailing winds, these aerosols substantially influence air quality across the Indo-Gangetic Plain. In this study, forward wind trajectory analysis further demonstrates that air masses originating in Punjab frequently move toward the IGP region, supporting the observed regional impact of CRB emissions.

Keywords: Crop residue burning, Black carbon, Optical properties, Punjab, Air pollution

1. Introduction

Black carbon (BC) is a refractory, light-absorbing carbonaceous aerosol produced primarily during the incomplete combustion of carbon-based fuels such as fossil fuels, biomass, etc (Bikkina et al., 2019; Bisht et al., 2015; Bond et al., 2011). It is well known for its high light-absorbing properties, which make it the second most warming species in the atmosphere after CO_2 (Bond et al., 2013). The Intergovernmental Panel on Climate Change (IPCC) recognises BC as a significant contributor to global warming, primarily due to its positive radiative forcing (RF), which enhances atmospheric warming (IPCC, 2023). Recent simulations of global climate models suggest that BC could potentially increase the global average surface temperature by 0.4–0.5 °C. Its size ranges from a few nanometres to micrometres (Gong et al., 2016; Goel et al., 2020; Zhang et al., 2019) and can travel deep into our respiratory system and cause cardiovascular and pulmonary diseases; because of these properties, BC also made its way into the COP28 agenda, where 198 nations agreed to transition away from fossil fuel to reduce BC emissions, a short-lived pollutant (SLP), having a lifetime of about 4-7 days in the atmosphere. Therefore, a reduction in BC emissions can result in immediate results. The rapid pace of economic development, industrial expansion, urbanisation, and rising energy consumption, coupled with widespread and often unregulated biomass burning, including agricultural residue, peat, and forest fires, has led to a significant increase in black BC emissions across South and East Asia.

In this study, the BC is monitored over a village during the active Crop residue burning (CRB) events during the post-monsoon season. This emits BC and other pollutants in large amounts and deteriorates the air quality of the Indo-Gangetic Plain (IGP) region. The Air Quality Index (AQI) of the IGP region is predominantly measured at hazardous levels when the crop residue is burned in the fields. This reduces visibility and elevated health issues in the inhabitants of the IGP region. Every year, the government impose a ban on these activities and implements

policies to improve the air quality of the region, but still it is measured in the hazardous category.

Multiple studies have identified Delhi, a major metropolitan centre, as one of the most polluted cities globally, deteriorating significantly during post-monsoon due to stubble burning in the neighbouring upwind states of Punjab and Haryana. This seasonal phenomenon contributes to the already challenging pollution levels in the region, exacerbating health risks and environmental concerns for residents (Dumka et al., 2018; Goel et al., 2021a).

Different approaches are employed for identifying sources of BC, including (i) the carbon isotope (14C) method (Gustafsson et al., 2009), the Aethalometer model (Sandradewi et al., 2008), (ii) the macro tracer method (Reche et al., 2015) (Viana et al., 2013), (iii) the chemical mass balance model (Favez et al., 2010), (iv) the positive matrix factorization (PMF) model (Kumar et al., 2024), and (v) climate simulation techniques (Yang et al., 2018), such as the WRF-Chem model, each possessing distinct pros and cons. The outcomes of these techniques may vary due to the limitations and assumptions associated with each approach (Viana et al., 2008). For instance, the carbon isotope (14C) method is capable of directly quantifying the relative contributions of biomass burning and fossil fuel combustion to black carbon (BC) concentrations. However, this approach is constrained by its limited temporal resolution (Chen et al., 2013). Furthermore, numerous source apportionment (SA) techniques, such as the Aethalometer model (AM), macro-tracer method, and radiocarbon method, exhibit limitations in accurately distinguishing and allocating contributions from two major BC sources: fossil fuel combustion and biomass burning (Briggs and Long, 2016). These limitations arise from the inherent assumptions and methodological constraints associated with each technique, which can affect the precision and reliability of source attribution. Aethalometer models are widely utilized for the bifurcation of BC around the globe (Dumka et al., 2019, 2018; Goel et al., 2023a, 2021b; Herich et al., 2011; Mousavi et al., 2018; Sandradewi et al., 2008; Tiwari et

al., 2013; Vaishya et al., 2017). (Kumar et al., 2024) recently implemented two approaches, AM and PMF models, for BC source apportionment over the Delhi region.

The objective of this study is to investigate ambient black carbon (BC) levels and assess their dependency on biomass burning during the post-monsoon season, a period marked by intense crop residue burning in Punjab. To achieve this, BC concentrations were measured and analysed using both the Aethalometer Model (AM) and Positive Matrix Factorization (PMF) to apportion contributions from various emission sources. While the AM offers real-time source attribution based on optical properties, it is limited by its assumption of fixed wavelength-dependent Angstrom exponent values and its two-source resolution. In contrast, the PMF model provides a more comprehensive and flexible framework capable of resolving multiple BC sources. Additionally, the absorption properties of BC and brown carbon (BrC), including the average Absorption Angstrom Exponent (AAE), were analysed to gain further insight into the optical characteristics of biomass-burning carbonaceous aerosols.

This study will assist policymakers in understanding the sources and extent of BC emissions during the crop residue burning period, enabling the development of targeted mitigation strategies to reduce BC levels and improve ambient air quality in the region.

2. Material and methodology

2.1. Sampling sites:

A stubble burning campaign (STUB-BURN) was conducted in Punjab to study aerosols emitting from biomass burning at a community health centre in Khera Village (30.604312, 76.489195). The sampling site was in a rural area surrounded by agricultural fields and is situated near a connecting road between State Highway 12A and National Highway (NH44), both approximately 5 km from the site. Additionally, the Rajpura Thermal Power Plant is

147 located about 10 km away. The geographical coordinates and layout of the site are presented in
148 Supplementary Information Figure S1. The instruments were housed in a temperature-
149 controlled mobile laboratory called the Clean Air Research Laboratory (CARLab). The STUB-
150 BURN campaign was conducted from October 27th – November 18th 2023. Wind at the
151 sampling site was majorly coming from the north-west direction. The biomass-burning (bb)
152 events were predominantly observed near to the sampling site till November 9th after that
153 significant decrease in such events was observed near to the site. However, the NASA FIRMS
154 data confirmed bb in other parts of Punjab and Haryana. Diwali, a major cultural festival in
155 India, was celebrated on November 12, 2023, and is typically associated with an extensive
156 firecracker event, resulting in a sharp and short-term increase in atmospheric particulate matter
157 and trace gas concentrations.

158 **2.2. Instrumentation:**

159 Black carbon (BC) measurements were conducted with a seven-wavelength Aethalometer
160 (AE33; Magee Scientific®), which provides real-time data based on differential optical
161 absorption. The light attenuation was measured at 370, 470, 520, 590, 660, 880, and 950 nm.
162 The optical attenuation measured by the Aethalometer is proportional to the amount of BC
163 deposited on the filter tape and is subsequently converted to equivalent BC concentration. The
164 loading and shadowing effects are taken care of by introducing a correction factor in the
165 measurements. The Aethalometer employed in this study utilizes dual-spot technology, which
166 divides the incoming aerosol-laden airflow into two unequal streams for improved
167 compensation of filter loading effects. Particles are collected on a quartz filter tape through a
168 $PM_{2.5}$ inlet, positioned approximately 3 meters above ground level. Moisture in the sample air
169 was removed using a Nafion dryer, installed upstream of the aethalometer. It was operated at a
170 constant volumetric flow rate of 2 L min^{-1}, providing high-time-resolution BC measurements

at 1-minute intervals. The instrument was calibrated before the campaign following the protocol suggested by the manufacturer and Cuesta-Mosquera et al., 2008.

The real-time elemental composition of $PM_{2.5}$ was analysed using the Xact 625i ambient metals monitor (Cooper Environmental®), which provides high-resolution, time-resolved measurements. The $PM_{2.5}$ samples were collected over a Teflon tape, and the elemental composition was measured at a resolution of 30 min. The flow rate was maintained at 16.67LPM. The inlet was installed approximately 3 m above the ground. The instruments calibrated itself automatically daily between 00:00-00:30hrs. This instrument works on Energy Dispersive X-ray Fluorescence Spectroscopy (EDXRF), where the sample is illuminated with X-rays, which excite the inner core electrons to an excited state. After excitation, the electrons return back to their ground state and release the absorbed energy in the form of X-rays that are detected by the detector. The released X-rays are the characteristic property of every element and work as a fingerprint for element identification. The amplitude of the signal helps in the quantitative analysis of elements. Xact is a widely used instrument for the real-time elemental analysis of aerosols. Detailed information on the instrument's operating principle can be found in the existing literature (Epa, 2013). Meteorological parameters, including wind speed and wind direction, were measured using an ultrasonic wind sensor (WindSonic; Gill Instruments®), while ambient temperature and relative humidity (RH) were monitored using a temperature-RH sensor integrated with the Xact instruments.

2.3. Source apportionment methodology:

2.3.1. Aethalometer Model:

The wavelength dependence of aerosol absorption follows a power-law relationship, represented by Equation (1), while the absorption Ångström exponent (AAE) between two wavelengths is calculated using Equation (2).

$$b_{abs}(\lambda) \sim \lambda^{-\alpha} \quad (1)$$

$$\frac{b_{abs}(\lambda_1)}{b_{abs}(\lambda_2)} = \left(\frac{\lambda_1}{\lambda_2}\right)^{\alpha} \quad (2)$$

Where λ is the wavelength and α is the Absorption Angstrom Exponent.

BC absorbs solar radiation in the wide spectrum from the NUV – NIR region with weak spectral dependence α ~ 1. The fossil fuel combustion mainly contains BC and basically no other compound, so the α for ff is ~1. In contrary, the bb emissions consist of substantial amount of light absorbing organic compounds along with the BC, that absorbs strongly in the NUV region, in the blue spectrum, and have negligible absorbance in the NIR region. Therefore, α for bb is higher than 1. Based on this, the aethalometer is developed, which bifurcates BC into two sources: biomass burning (bb) and fossil fuel combustion (ff), assuming that total absorption is dependent on these two sources only (Sandradewi et al., 2008).

$$b_{abs} = b_{abs}(ff) + b_{abs}(bb) \quad (3)$$

The apportionment into fossil fuel combustion and biomass burning was done using the eq. 3-5 and b_{abs}.

$$\frac{b_{abs,ff,\lambda_1}}{b_{abs,ff,\lambda_2}} = \left(\frac{\lambda_1}{\lambda_2}\right)^{-\alpha_{ff}} \quad (4)$$

$$\frac{b_{abs,bb,\lambda_1}}{b_{abs,bb,\lambda_2}} = \left(\frac{\lambda_1}{\lambda_2}\right)^{-\alpha_{bb}} \quad (5)$$

Aethalometer model is used globally for BC source apportionment, in a variety of regions varying from pristine to a typical urban environment. The model was developed in Europe for a region with defined BC sources such as wood burning and traffic emissions, but later on it was used globally in environments with mixed sources. The diversion could incorporate uncertainty in estimations, but still, this is a very simple and reliable model for real-time source apportionment of BC. (Sandradewi et al., 2008) and other studies used 470 and 950 nm

wavelength pair for BC source apportionment. Different studies also used 370 and 880, or 470 and 880 wavelength pairs. In the present study, the 370 and 950 nm wavelength pair is used.

2.3.2. Positive Matrix Factorization (PMF) model:

In this study, the PMF model, initially developed by Paatero and Tapper (1994) , was employed to elucidate the sources BC observed during the Punjab campaign, conducted in close proximity to active stubble-burning sites. PMF is a complex multivariate statistical tool that separates the factors based on the covariance of the different species. This model is widely employed to estimate the sources of ambient particulate matter (PM) (Faisal et al., 2025, 2024; Manchanda et al., 2021; Sharma et al., 2016; Shukla et al., 2021; Ulbrich et al., 2009; Vossler et al., 2016) . The algorithm of this model employs a least squares approach to decompose the data matrix into two distinct matrices: a source profile matrix and a source contribution matrix, as mathematically represented in Equation 6.

$$X_{ij} = \sum_{k=1}^{p} g_{ik} f_{kj} \quad (6)$$

In the model, X_{ij} represents the ambient concentration of elemental species, f_{kj} denotes the source profile, g_{ik} reflects the contribution of each source at a given time step, and e_{ik} corresponds to the residual matrix. Here, the indices i and j refer to the n time steps and m chemical species, respectively, while k represents each of the p source profiles or the number of factors specified by the user. This framework allows for systematically identifying and quantifying emission sources based on their chemical signatures and temporal contributions. The Positive Matrix Factorization (PMF) model incorporates a non-negativity constraint through penalty functions, ensuring that source contributions remain physically meaningful. It solves the bilinear model using a weighted least squares approach that minimizes an objective function (Q), defined as the sum of the squared ratios of residuals (e_{ij}) to their associated uncertainties (σ_{ij}). Mathematically, the objective function is represented as equation 7:

$$Q = \sum_i \sum_j \left(\frac{e_{ij}}{s_{ij}}\right)^2 \quad (7)$$

In equation (7), s_{ij} denotes the measurement uncertainty for each cell of the input matrix x_{ij}. The current study employed the PMF algorithm utilizing EPA PMF 5.0, which is based on the ME-2 solution model. A comprehensive explanation of the PMF model is presented in previous research. (Paatero, 1999; Paatero and Tapper, 1994). The present study implemented the coupled PMF method, initially proposed by (Petit et al., 2014). BC concentration data has been combined with the elemental tracer to perform the coupled PMF. The study utilized elemental concentration data obtained from the Xact 625i instrument and black carbon (BC) measurements from an aethalometer as inputs for the PMF model. Detailed methodologies regarding the preparation of PMF inputs, the selection of factors, and the quantification of uncertainties for the coupled PMF analysis are provided in Supplementary Material S2.

2.4. Aerosol Absorption properties:

The absorption properties of the BC and brown carbon (BrC) were estimated using the approach discussed in Lack and Langridge 2013. Mass absorption cross-section (MAC) values at wavelengths of 370, 470, 520, 590, 660, 880, and 950 nm were specified by the instrument manufacturer, with corresponding values of 8.47, 14.54, 13.14, 11.58, 10.35, 7.77, and 7.19 $m^2\ g^{-1}$, respectively. The total absorption was attributed to BC and BrC only with an assumption of no absorption from dust eq (8).

$$\mathrm{Abs}\ (\lambda) = \mathrm{Abs}\ (\lambda)_{BC} + \mathrm{Abs}(\lambda)_{BrC} \quad (8)$$

$\mathrm{Abs}(\lambda)_{BC}$ and $\mathrm{Abs}(\lambda)_{BrC}$ are absorption from BC and BrC at wavelength (λ), respectively. Another assumption in this approach is being BC the only absorber at 880nm and above, thus $\mathrm{Abs}(\boldsymbol{\lambda})_{BC}$ at 370, 470, 520, 590, 660nm was calculated using equation 9.

$$\mathrm{Abs}(\lambda)_{BC} = \mathrm{Abs880} * \left(\frac{\lambda}{880}\right)^{-AAE_{BC}} \quad (9)$$

AAE_{BC} is considered as 1 based on the literature (Lack and Langridge 2013; Wang et al. 2019; Li et al. 2022). Therefore, $AAE(\lambda)_{BrC}$ at 370, 470, 520, 590, 660nm was calculated using equation 10.

$$Abs(\lambda)_{BrC} = 1 - Abs880 * \left(\frac{\lambda}{880}\right)^{-AAE_{BC}} \quad (10)$$

Absorption Angstrom Exponent was calculated for the 370, 880 nm wavelength pair using absorption coefficient, product of MAC and BC concentration (eq. 11 and 12).

$$b_{abs} = BC \times MAC \quad (11)$$

$$AAE = -\frac{\ln(b_{370}/\, b_{880})}{\ln(370/880)} \quad (12)$$

Here, b370 and b880 represent the measured absorption coefficients at wavelengths of 370 nm and 880 nm, respectively.

2.5 Forward wind trajectory analysis

In the present study, 72-h forward wind trajectories were computed from the agricultural regions of Punjab and Haryana over the north-western Indo-Gangetic Plain (IGP) during October–November 2023 to investigate air-mass transport toward the central IGP and the National Capital Region (NCR), Delhi. These months correspond to the post-monsoon season, which is characterized by extensive stubble-burning activities in northwestern India. The trajectories were computed at a height of 100 m above mean sea level (amsl) using the Hybrid Single-Particle Lagrangian Integrated Trajectory (HYSPLIT) model, developed by the National Oceanic and Atmospheric Administration (NOAA) Air Resources Laboratory (ARL), with Global Data Assimilation System (GDAS) meteorological data as input.

The forward wind trajectory is shown in Figure 1, depicting the trajectories that move toward the IGP region from Punjab. The forward trajectories clearly indicate that air parcels originating over the crop-residue burning regions of Punjab and Haryana were frequently transported towards IGP and the Delhi megacity during the study period. The dominant wind flow during this period was predominantly from the northwestern sector, which facilitated the long-range transport of smoke-laden air masses over the Indo-Gangetic Plain and into the NCR. These air masses carried a significant load of particulate matter and black carbon (BC) originating from the open burning of agricultural crop residues. Similar findings on the contribution of crop residue burning to Delhi's deteriorating air quality during the post-monsoon period have been reported in previous studies (Bikkina et al., 2019; Jain et al., 2020).

3. Results and discussions

3.1. Temporal and diurnal variation of BC

The black carbon (BC) concentration derived at 880 nm is considered a reliable estimate of true BC, as the absorption contribution from other aerosol species such as mineral dust and organic carbon is negligible at this near-infrared wavelength. The study averaged BC concentration was 12.6 $\mu g/m^3$ ranging from 1.45 – 85.0 $\mu g/m^3$ on a minute scale. The measured BC concentration is lower than the values reported over Delhi during the post-monsoon season by Goel et al. (2023a), which was 17.23 $\mu g/m^3$ in 2022, and by Goel et al. (2021a), which was 19.1 $\mu g/m^3$ in 2020. However, it is comparable to the concentration reported over Agra by Gupta et al. (2017), approximately 13.0 $\mu g/m^3$ in 2014. The BC concentration measured in this study is substantially high, posing serious threat to the inhabitants. The temporal variation of BC concentration is shown in Figure 2a. The 24-hour averaged BC concentration varied from 6.2 – 17.3 $\mu g/m^3$, reaching its lowest level on November 10th. This decrease can be attributed to rainfall on that day, which facilitated wet deposition, effectively reducing BC levels in the region. Conversely, the highest concentration was recorded on November 1st, aligning with intense biomass burning events occurring near the sampling site. The study period can be bifurcated into two distinct phases: from October 27th to November 9th, and from November 10th to November 18th. During phase 1, bb events were notably intense at the sampling site in comparison to phase 2, resulting in very high BC concentration. Specifically, the BC concentration during phase 1 averaged at 14.5 $\mu g/m^3$. In contrast, during phase 2, the intensity of bb events was very minimal, reflected in a decrease in BC concentration to an average of 9.7 $\mu g/m^3$. The diurnal variation of BC shown in Figure 3d represents highest BC concentration around 21:00 and lowest around 13:00. The Figure is illustrated with three distinct peaks, representing elevated BC concentration around 07:00, 19:00, and 21:00.

3.2. Temporal variation of AAE:

The temporal and diurnal variations of AAE are shown in Figures 2b and 3b, respectively. The study average AAE was 1.7 ± 0.3, ranging from 1.1 – 2.4 on an hourly scale. During Phase 1, the AAE was 1.76 ± 0.29, while during Phase 2, it was 1.56 ± 0.24. The higher AAE observed in phase 1 was the influence of intensive bb activities, leading to a higher AAE compared to phase 2. The lowest daily average AAE was observed on November 10th, attributed to the rain events at the sampling site and neighbouring states. The highest daily averaged AAE was observed in phase 1 on the 2nd, 3rd, and 5th of November, i.e., 1.82, 1.88, and 1.88, respectively. The high AAE results from intensive biomass-burning activities near to the sampling site. The AAE observed in present study is higher than Goel et al. (2021a) (i.e., 1.30 ± 0.16), Goel et al. (2020) (i.e., 1.32 ± 0.16), Dumka et al., (2018) (i.e., 1.29 ± 0.08), Tiwari et al. (2015) (i.e., 1.09 ± 0.11) but lower than reported by Ganguly et al. (2006) (i.e., 1.9 ± 0.1). The observed AAE is similar to what was observed in Roveredo for the winter period, i.e., 1.6 ± 0.2 for the 370 and 950 nm wavelength pair. The higher AAE in the present study is attributed to the enhanced contribution of biomass burning aerosols at the sampling site (Reddy and Venkataraman, 2002). Biomass burning aerosols exhibit strong absorption in the UV region, which significantly decreases in the IR region. This characteristic results in a high AAE, reaching values up to approximately 2 for pure biomass burning aerosols (Kirchstetter et al., 2004; Schmid et al., 2006).

The diurnal variation of AAE exhibit strong variation ranging from 1.33 (09:00 – 10:00) – 1.97 (22:00) on an hourly scale. The variation is attributed to the variation in bb and ff combustion sources diurnally. During the early morning hours, lower AAE values (around 1.33) suggest a higher contribution from fossil fuel combustion, which typically has a lower AAE. This is likely due to increased vehicular and industrial activities during the morning commute. As the day progresses, the relative contribution from biomass burning, which generally has a higher

AAE, increases. This could be due to various factors such as agricultural practices, cooking, and other local biomass burning activities that intensify later in the day. By late evening, the highest AAE value (1.97 at 22:00) indicates a strong influence of biomass burning sources. This may be due to the accumulation of particles that emitted throughout the day and evening from agricultural burning and cooking sources. Overall, the diurnal pattern of AAE reflects the dynamic interplay between different combustion sources, with fossil fuel emissions dominating in the morning and biomass burning emissions becoming more prominent in the evening.

3.3. Absorption properties:

The absorption properties of black carbon (BC) and brown carbon (BrC) during the campaign are depicted in Figure 4. The absorption coefficients (b_{abs}) at wavelengths of 370, 470, 520, 590, 660, 880, and 950 nm were measured as 595.85, 382.50, 279.23, 265.93, 227.01, 148.14, and 137.23 mm^{-1}, respectively. The contributions of BC and BrC to total absorption varied across these wavelengths. At 370 nm, BC contributed 59.13% and BrC 40.87%, indicating substantial UV absorption by BrC. This high BrC contribution in the UV range is likely due to the presence of organic compounds, such as humic-like substances (HULIS), which are characteristic of biomass burning emissions and are known for their strong absorption in the UV and blue regions of the spectrum.

As the wavelength increased, the contribution of BC became increasingly dominant. At 470 nm, BC accounted for 72.52% of absorption, and at 520 nm, this rose to 79.13%. By 590 nm, BC's contribution reached 94.27%, with BrC's influence reduced to 5.73%. This shift indicates the decreasing impact of BrC as the wavelength moves from the UV to the visible spectrum, aligning with BrC's characteristic decline in absorption efficiency at longer wavelengths. At 660 nm, BC contributed 87.01%, while BrC contributed 12.99%. In the near-infrared regions

of 880 and 950 nm, BC's contributions were 100%, with no measurable contribution from BrC and this was due to the assumption discussed in section 2.4. This dominance of BC in the near-infrared region is consistent with its broad-spectrum absorption capability, attributed to its graphitic and elemental carbon structure that absorbs efficiently across a wide range of wavelengths. The variation in the absorption properties between BC and BrC has significant implications for understanding the radiative forcing effects of these aerosols. BC's strong absorption across the visible and near-infrared spectrum contributes to warming effects by reducing the albedo when deposited on snow and directly heating the atmosphere. In contrast, BrC, with its substantial UV absorption, affects photochemical processes and can alter atmospheric chemistry by influencing the formation of secondary organic aerosols (SOA) and other photochemical products. In summary, the data underscores the distinct and complementary roles of BC and BrC in atmospheric absorption. BC is the predominant absorber in the visible and near-infrared regions, while BrC significantly impacts the UV and blue regions. These differences highlight the need for detailed characterization of both types of aerosols to fully understand their environmental and climatic impacts.

3.4. Source apportionment:

3.4.1. Aethalometer model:

Aethalometer model has an intrinsic limitation to apportion BC into only two sources such as biomass burning and fossil fuel combustion. The apportionment is done assuming AAE values as 1 for ff and 2 for bb. The assumption is based on the previous studies and the dominant BC sources present at the sampling site. The results represent significant temporal and diurnal variations in BC_{bb} and BC_{ff} concentrations during the study period. The temporal variation of BC_{bb} and BC_{ff} is shown in Figure 2c. The study averaged BC_{bb} concentration was 6.22 ± 4.64

μg/m³, ranging from 0.50 – 26.45 μg/m³ on an hourly scale, and BCff was 6.59 ± 2.76 μg/m³, ranging from 0.71 – 17.11 μg/m³ on an hourly scale. The lowest 24 hours averaged BC_{bb} concentration was observed on November 11th and highest on November 1st. The site experienced rain on November 10th, which wet the agricultural waste residue. As a result, farmers were unable to burn the residue on November 11th, leading to a reduction in the BC_{bb} concentration. The BC_{bb} concentration during the phase 1 was 7.7 ± 5.2 μg/m³ ranging from 1.46 – 26.45 μg/m³ and during phase 2 it decreased to 3.57 ± 2.28 μg/m³ ranging from 0.50 – 12.84 μg/m³ on hourly scale. Whereas the BC_{ff} concentration during phase 1 was 6.79 ± 2.65 ranging from 1.3 -17.11 μg/m³ and during phase 2 was 6.26 ± 2.91 μg/m³ ranging from 0.71 - 16.45 μg/m³, on hourly scale. The BC_{ff} concentration seems not to vary much because the vehicular emission was consistent during both the phases. The contribution of BC_{bb} and BC_{ff} during phase 1 was 54% and 46% and during phase 2 was 36 and 64%, respectively. The results revealed clear difference in source strengths between phase 1 and 2, where bb is a major source in phase 1 and ff in phase 2.

In spite of the sampling being done in the middle of the agricultural fields during the bb activities, the ff combustion contributed 51.5% and bb contributed 48.5% to the total BC. The contribution of ff is slightly higher than bb and quite similar to what is reported in Delhi i.e., bb (51%) and ff (49%) during the post-monsoon season in year 2022 (Goel et al., 2023a). The results revealed no significant difference in the contribution of bb and ff to the BC concentration over the study site. This can be explained with the diurnal variation of bb and ff sources strengths. The diurnal variation of BC_{bb}% and BC_{ff}% is shown in Figure 3a and 3c. Diurnally, the BC_{bb}% varied from 23.54 – 92.62 % and BC_{ff}% varied from 7.38 – 76.46% on a minute scale. The diurnal variation showed that from 3:00 till 14:00 BC_{ff} is the dominant source and from 14:00 to 03:00 BC_{bb} dominated the BC concentration. The BC_{bb} variation aligns with the variation in bb events at the site. The bb markers (shown in the later section)

concentration starts increasing around 13:00 every day and dips by the sunset (around 18:00). The BC_{bb} concentration starts increasing around 12:00, peaked around 22:00 and then starts decreasing and reached its minimum value in morning around 09:30 and stayed at that level till 12:00. At 22:00 no agricultural waste residue burning was observed still the BC_{bb} was at its peak, this can be attributed to the decrease in planetary boundary layer height (PBLH) and increase in bb activity for cooking purpose. In rural areas of India, biomass fuels like wood and cow dung patties are commonly used to cook food during the morning and evening hours, which increases the BC_{bb} concentration. The BC_{bb} concentration was minimum between 9:30 – 12:00 because of absence of bb events and fully evolved PBLH. The diurnal variation of BC_{bb} observed in the present study displayed a distinct pattern compared to what has been documented in Delhi and other studies in the literature (Ambade et al., 2021; Dumka et al., 2018; Goel et al., 2021a and 2023a; Tiwari et al., 2013). While in Delhi and other locations the BC_{bb} concentration is reported to be lowest in the afternoon (around 15:00), in the present study, the lowest concentration was observed at 09:30. This unique feature is influenced by the diurnal variation of biomass burning activities in the proximity of the sampling site.

Potassium (K) is widely recognized as a tracer for biomass burning (BB) emissions and is typically present in the form of potassium chloride (KCl). In this study, real-time concentrations of K were measured using the Xact instrument and compared with biomass burning-derived black carbon (BC_{bb}), as shown in Supplementary Figure S2. A strong positive correlation (r^2 = 0.71) was observed between K and BC_{bb} across the study region, supporting the validity of the aethalometer-based source apportionment results.

3.4.2. Black Carbon source allocation using coupled PMF

This section describes a coupled PMF analysis, combining elemental data obtained from the Xact 625i with BC concentrations measured using the AE33. Trace elements were utilized as tracers to effectively apportion BC sources. From the initial set of 36 measured elements, 15 elements, along with BC, were chosen for the input matrix in the PMF model. Specific elements were excluded to enhance the model's robustness, as their contributions exhibited weak correlations between the measured species and those predicted by the PMF model, as outlined in Supplementary Section S2. The PMF analysis resolved a six-factor solution, identifying key sources, including biomass burning, traffic emissions, power plants, dust-related, waste incineration, and a Pb-rich factor. Among these, five factors were identified as major contributors to BC. Resolved factors were identified by analysing the presence of specific marker species within each factor. Diurnal and temporal variation patterns were also examined to determine the most plausible sources. Biomass burning was identified as the predominant source of BC, contributing 47.7% of the total BC concentration. The temporal variation of BC sources derived from the PMF model was quantified by normalising PMF factors based on the percentage of BC mass within each factor. BC coming from biomass burning, vehicular emissions, power generation, waste incineration, and Pb-enriched sources was denoted as BC_{BB}, BC_{VE}, BC_{PP}, BC_{WI}, and $BC_{Pb-rich}$, respectively. Analysing the dominant species within each factor profile determined source attribution for each resolved factor. The contributions of each species were quantified using two analytical approaches:

1. Factor-specific contribution: Calculated as the percentage of the total factor mass, determined by the ratio of the average concentration of the target species to the sum of the average concentrations of all species within the factor.

2. Species distribution across factors: Determined as the percentage of the species concentration in the given factor relative to the total concentration of that species across all factors.

Out of the six resolved factors, five have been identified as significant sources of BC. The factors associated with biomass burning, traffic emissions and power plant are discussed below, while the rest are discussed in the Supplementary information section S3.

3.4.2.1. Biomass burning

The chemical fingerprint of this factor shown in Figure 6a, characterized by elevated levels of BC, K, Cl, Se, Si, and S, is consistent with previously reported markers associated with biomass burning (Dumka et al., 2019; Jiang et al., 2024; Sandradewi et al., 2008). In terms of factor mass contribution, BC dominated this factor (57.5%), followed by chlorine (Cl, 27%), potassium (K, 12.5%), selenium (Se, 2%), and sulphur (S, 2%). Further analysis of the percentage distribution of individual species across all identified factors revealed that this factor contributed 81% of the total Cl, 69% of Se, 58% of bromine (Br), 47.7% of BC, 40.5% of K, 6.7% of Si, and 5% of S. High percentage of K along with BC identified this factor as a biomass burning factor. Numerous studies worldwide have utilized potassium (K) as a key elemental tracer for identifying biomass burning sources (Khare et al., 2011; Manchanda et al., 2021; Pant and Harrison, 2012; Reche et al., 2015; Shukla et al., 2023). Potassium is widely recognized as a reliable tracer for biomass burning due to its consistent presence in combustion emissions, making it a key indicator for identifying biomass-related contributions in source apportionment studies. During the study period, a strong correlation was observed between elemental K and BC, with a Pearson correlation coefficient of r = 0.75 (Figure S6b). This significant relationship suggests a common emission source for both species, likely stubble

burning. The high presence of chlorine (81% of the total Cl measured) at the sampling site, surrounded by farmland, suggests that fresh biomass burning is a key source of chlorine. The strong correlation between K and Cl concentrations (Pearson coefficient, r = 0.83), as shown in Figure S6a, further supports this common source. Multiple studies have reported that potassium primarily exists as potassium chloride (KCl) in fresh biomass-burning plumes. In aged plumes, sulfates partially substitute chlorides, indicating elevated chloride levels associated with potassium from biomass-burning sources (Chang et al., 2024; Li et al., 2003). Previous research has reported substantial biomass growth in selenium-enriched soils (Furger et al., 2017; Soltes and Elder, 1981), which are prevalent in northern India (Sharma et al., 2009). Additionally, the combustion of fibrous biomass, such as straw, cereal, and grass, has been identified as a Si source (Obernberger et al., 2006).

The mean BC emitted from this factor (BC_{BB}) was 5.40 ug/m^3 during the crop residue burning (CRB). The concentration of this factor begins to rise in late October and reaches its peak in the first week of November, aligning with the paddy harvesting period. This time period corresponds to an increase in CRB activities (Jethva et al., 2019).

511 The diurnal variation of the BC factor attributed to biomass burning (BC_{BB}), as shown in Figure
512 5a, reveals low daytime concentrations, with a minimum of 3 μg/m^3 observed at 13:00 hours.
513 This reduction during daytime is associated with a well-developed planetary boundary layer
514 height (PBLH), which enhances vertical mixing and dispersion of pollutants. In the evening,
515 as the PBLH decreases and atmospheric stability increases, BC_{BB} concentrations rise, reaching
516 a 12 μg/m^3 peak at 20:00 hours. This evening peak reflects reduced dispersion and increased
517 emissions from biomass-burning activities, which are often more prevalent during the evening
518 hours.

519 **3.4.2.2. Traffic emission**

520 The traffic emission source (Figure 6c) was found to be dominated by BC (80%) in terms of
521 the % factor mass, followed by Fe (6.23%), S (6%), and Zn (2.5%), respectively. However, in
522 terms of the % species across factors, traffic emission factor accounted for 52.38% of total Cu,
523 43.2 % of total Fe, 38% of the total Mn content, followed by 32.4% of total Si, 17% of BC,
524 15% of Cr, 12% of As, 6% of Zn, and 4% of S. Prior studies have indicated that the elements
525 found in this factor profile, including BC, Cu, Fe, Mn, Cr, As, Zn, and Sb, act as indicators of
526 traffic emissions. Black carbon is primarily released through the combustion of fossil fuels
527 (Freitas et al., 2021; Sandradewi et al., 2008). Sulphur naturally exists in crude oil; although
528 pollution control efforts have primarily targeted the reduction of sulfur levels in fuels, research
529 has highlighted sulphur application in engine oil's anti-wear additives (Fitch, 2019). Numerous
530 investigations conducted previously have linked Mn, Fe, Zn, and Fe to emissions from vehicles,
531 as well as wear from brakes and engines, identifying these elements as prevalent trace
532 components in brake pads and linings (Faisal et al., 2024; Grigoratos and Martini, 2015; Rai et
533 al., 2020; Thorpe and Harrison, 2008). Van der Gon et al. (2007) have reassessed the Cu
534 emissions due to exhaust emissions and brake wear from road transport. The average
535 concentration of BC associated with this factor (BC_{VE}) was 2.30 ± 1.95 μg/m³.

The diurnal variation of the BC_{VE} factor, as shown in Figure 5c, exhibits a distinct early morning peak followed by an increase in the evening, with a peak value of 3 μg/m^3 around 7:00 hours. This pattern aligns with typical traffic rush hours, where increased vehicular activity leads to BC levels. The morning peak likely reflects public and diesel-heavy transport during the start of the day, while the evening rise corresponds to increased traffic volumes associated with end-of-day travel activities.

3.4.2.3. Power plant

The power plant factor is recognized by a high abundance of BC (46%), S (35%), and K (16%) in terms of factor mass contribution (Figure 6b). It accounts for 68.5% of S, 37% of K, 31% of Ti, 51% of As, 12.4% of Fe, 27% of BC, 26% of Se, and 21% of Br in terms of species contribution. Previous studies have identified As and Se as key tracers of power plant emissions associated with coal combustion (Sloss, 2012, Monaghan et al., 2009; Kumar, M. 2011). This factor contributes 27% to the total BC mass in this analysis, with an average BC level of 2.72 μg/m³. Rai et al. (2020) reported that sulphur in $PM_{2.5}$ primarily exists as secondary sulfate. Several coal-fired power plants, including the Guru Gobind Singh thermal power plant, are operational in Punjab and Haryana, likely contributing to the observed power plant factor. The Rajpura thermal Power plant is situated near the receptor site, only 10 km away. This factor is identified as a significant source of BC emissions following stubble burning. This is attributed to several power plants in Punjab and Haryana that utilize crop residue (stubble) as fuel. The combustion of stubble in these power plants generates significant BC emissions, contributing notably to ambient BC levels at the site. Chauhan, 2010 estimated a considerable availability of biomass resources, predominantly crop residue, and sawdust, in Haryana, with a power generation potential exceeding 1 GW. A significant portion of this potential appears to have been realized in subsequent years. Recent policy initiatives have further accelerated the use of biomass in thermal power plants. In 2023, the Ministry of Power issued directives (R.I.

1945245, 2023) mandating a 5% blending of biomass pellets in thermal power plants (Ministry of Power directives, 2023). The Ministry of New and Renewable Energy (MNRE) also reported operational capacities for biomass-based power generation in Haryana and Punjab at 240.66 MW and 481.15 MW, respectively (Kumar et al., 2024). These findings highlight the growing reliance on biomass as a fuel source and underscore its role in regional BC emissions. The diurnal variation of the BC_{PP}, as shown in Figure 5b, exhibits a distinct pattern with lower concentrations during the early morning hours (around 5:00–10:00) and higher concentrations in the late afternoon and evening (after 15:00)

3.5. Total source apportionment (elements and BC fraction of $PM_{2.5}$)

Positive Matrix Factorization (PMF) was applied to the speciated $PM_{2.5}$ dataset, comprising elemental concentrations and BC fractions, to identify and quantify the dominant emission sources influencing air quality in a predominantly agricultural region of Punjab, India. Leveraging high-resolution chemical speciation measured directly within a crop residue burning (CRB) source region, the PMF model produced an optimal six-factor solution that resolves distinct source signatures and their contributions to the elemental and BC fractions of $PM_{2.5}$. Stubble burning emissions emerged as the dominant factor, contributing 41% of the total elemental and BC mass, underscoring the strong impact of CRB on local aerosol composition during the burning period. Additional factors included power plant emissions (30%), traffic-related sources (11%), waste incineration (7%), a Pb-rich industrial factor (7%), and a dust-related factor (4%).

3.6 Comparison of the AM and positive matrix factorization (PMF) Model for BC Source Apportionment

The Aethalometer Model (AM) apportions ambient black carbon (BC) into two primary source categories: biomass burning (BC_{bb}) and fossil fuel combustion (BC_{ff}) by using the differential

spectral dependence of light absorption in the ultraviolet (UV) and infrared (IR) wavelengths. During the Punjab field campaign, the AM attributed 48.5% of total BC to BC_{bb} and 51.5% to BC_{ff}, reflecting the concurrent influence of agricultural burning and fossil fuel emissions in the region. However, the AM is intrinsically constrained by its two-source framework and cannot resolve additional emission sources. Recent study conducted by Kumar et al. (2024), highlight that the model's performance may be limited in complex and highly polluted environments where multiple combustion sources overlap, leading to potential misattribution of BC between the two categories.In contrast, PMF provides a more comprehensive source apportionment by utilizing the covariant concept among co-emitted elemental tracers. Using PMF, five distinct sources of BC were identified during the Punjab campaign: biomass burning, fossil fuel combustion, usually identified by the AM model, and three additional sources: waste incineration, power plant, and a Pb-rich factor that the AM model could not resolve. The PMF approach offers enhanced diagnostic capability for source identification, especially in regions with diverse emission profiles. The contributions of BC across factors identified by the PMF model are as follows: biomass burning (47.7%), traffic emissions (20.2%), power plants (24%), waste incineration (2%), and a Pb-enriched factor (6.1%).

The diurnal and temporal variations in BC emissions from various sources were quantified by normalizing the PMF-derived factors associated with BC.. The PMF-resolved sources were further consolidated into three primary categories, BC_{bb} (biomass burning), BC_{ff} (fossil fuel combustion), and $BC_{Miscellaneous}$, to facilitate comparison between the AM and PMF models (Kumar et al., 2024). A comparison of different source contributions to BC level obtained from AM and PMF models is shown in Table 1.

The significance of potassium (K) as a tracer for biomass-burning sources has been highlighted in multiple studies. The biomass burning factor derived from the AM (BC_{bb}) and the Positive PMF model (BC_{BB}) exhibited significant correlations with potassium (K), with Pearson

correlation coefficients (r) of 0.78 and 0.88, respectively. The high correlation between BC_{BB} and K, compared to BC_{bb}, suggests that the AM model, which is limited to only two factors, may have resulted in the misallocation of BC_{bb}. The high correlation of BC_{BB} and K underscores the potential of the PMF model to more accurately resolve sources associated with biomass burning.

The factors derived from the Aethalometer model (AM) and the PMF model were compared by computing correlations between corresponding sources, depicted in Figures 7c and 7d. The BC factors, denoted as BC_{bb} (AM) and BC_{BB} (PMF), exhibited a strong correlation of 0.92, indicating good agreement between the two models in identifying biomass-burning sources. In contrast, the fossil fuel-related factors, BC_{ff} (AM) and BC_{FF} (PMF), showed a weaker correlation of 0.50.

This weaker correlation suggests that the AM model's simplification attributes all fossil fuel combustion to a single factor that overlooks the complexity of emissions from distinct sources such as vehicular traffic, power plants, and industrial processes. In comparison, as a more advanced multivariate approach, the PMF model resolves multiple emission sources independently, offering a higher resolution of fossil fuel-related contributions. This highlights the PMF model's enhanced capability to differentiate between overlapping sources, improving the precision of source apportionment technique for BC.

4. Conclusion and future work

This study provides comprehensive measurements of ambient black carbon (BC) levels at a crop stubble burning (CRB) site in Punjab during the post-monsoon season and investigates their dependency on biomass burning. The findings are important because the emissions have wide-ranging health impacts across the wider Indo-Gangetic Plains (IGP) region including the downwind metropolitan city of Delhi. This regional influence is validated through forward

wind trajectory analysis, which demonstrates that air masses originating from the Punjab CRB region frequently transport toward the IGP, reinforcing the potential large-scale impact of these emissions on downwind air quality. The average BC concentration observed at the sampling site during the study period was 12.6 μg/m³, with values ranging from 1.45 to 85.0 μg/m³. Using both the Aethalometer Model (AM) and Positive Matrix Factorization (PMF), a detailed source apportionment of BC was conducted. The results reveal a strong influence of agricultural biomass burning on ambient BC, with the AM attributing 48.5% of BC to biomass burning and 51.5% to fossil fuel combustion. In contrast, the PMF model offered a more refined resolution, identifying five distinct sources: biomass burning (47.7%), traffic emissions (20.2%), power plant emissions (24.0%), waste incineration (2.0%), and a Pb-rich industrial factor (6.1%). The temporal and diurnal variations of BC and its sources were analysed to gain deeper insight into the emission patterns during the campaign. The detailed source apportionment results of BC presented in this study reveal the impact of stubble burning on local air quality, contributing to the elemental and BC fractions of $PM_{2.5}$.

Additionally, the absorption characteristics of both BC and brown carbon (BrC) were analysed during the measurement campaign, providing insight into the optical properties of carbonaceous aerosols. The analysis revealed an average Absorption Angstrom Exponent (AAE) of 1.7 ± 0.3, with hourly variations from 1.1 to 2.4. The elevated AAE values reflect a strong influence of biomass burning on ambient carbonaceous aerosols at the study site which ultimately get convected downwind across the IGP region. This study demonstrates the strengths and limitations of the two models, with AM being restricted to a simplified two-source apportionment, while PMF offers a more detailed identification of multiple BC sources. Implementing the PMF model in this study facilitated a more precise and detailed source apportionment of BC sources. Importantly, this study represents the first to quantitatively assess the contribution of local stubble burning to highly time-resolved BC measurements in

India. Measuring BC mass concentration and assessing its dependence on biomass burning in rural Punjab is critical for informing targeted air quality management strategies and developing evidence-based emission control policies aimed at mitigating pollution from crop residue burning, not only Punjab but across the entire Indo-Gangetic Plain (IGP).

Acknowledgement:

The authors would like to thank collaborators Ravindra Khaiwal and Suman Mor, and the CHE Hospital, Khera administration, for permission to conduct measurements at their sampling site. We acknowledge the use of the Near Real-Time (NRT) VIIRS 375 m Active Fire product (VNP14IMGT) distributed by NASA FIRMS. The authors would also like to thank the NOAA Air Resources Laboratory for the HYSPLIT model, as well as the Global Data Assimilation System (GDAS) for the meteorological input data.

Funding:

The authors acknowledge the financial support received from the IRD Grand Challenge Project (Grant No. 428 IITD/IRD/MI01810G) at the Indian Institute of Technology Delhi, funded by the Ministry of Human Resource Development (MHRD), Government of India, which enabled the successful execution of this study.

Reference:

Ambade, B., Sankar, T.K., Kumar, A., Gautam, A.S., Gautam, S., 2021. COVID-19 lockdowns reduce the Black carbon and polycyclic aromatic hydrocarbons of the Asian atmosphere: source apportionment and health hazard evaluation. Environ. Dev. Sustain. 23, 12252–12271. https://doi.org/10.1007/s10668-020-01167-1

Bikkina, S., Andersson, A., Kirillova, E.N., Holmstrand, H., Tiwari, S., Srivastava, A.K.,

Bisht, D.S., Gustafsson, Ö., 2019. Air quality in megacity Delhi affected by countryside biomass burning. Nat. Sustain. 2, 200–205. https://doi.org/10.1038/s41893-019-0219-0

Bisht, D.S., Dumka, U.C., Kaskaoutis, D.G., Pipal, A.S., Srivastava, A.K., Soni, V.K., Attri, S.D., Sateesh, M., Tiwari, S., 2015. Carbonaceous aerosols and pollutants over Delhi urban environment: Temporal evolution, source apportionment and radiative forcing. Sci. Total Environ. 521–522, 431–445. https://doi.org/10.1016/j.scitotenv.2015.03.083

Bond, T.C., Doherty, S.J., Fahey, D.W., Forster, P.M., Berntsen, T., Deangelo, B.J., Flanner, M.G., Ghan, S., Kärcher, B., Koch, D., Kinne, S., Kondo, Y., Quinn, P.K., Sarofim, M.C., Schultz, M.G., Schulz, M., Venkataraman, C., Zhang, H., Zhang, S., Bellouin, N., Guttikunda, S.K., Hopke, P.K., Jacobson, M.Z., Kaiser, J.W., Klimont, Z., Lohmann, U., Schwarz, J.P., Shindell, D., Storelvmo, T., Warren, S.G., Zender, C.S., 2013. Bounding the role of black carbon in the climate system: A scientific assessment. J. Geophys. Res. Atmos. 118, 5380–5552. https://doi.org/10.1002/jgrd.50171

Bond, T.C., Zarzycki, C., Flanner, M.G., Koch, D.M., 2011. Quantifying immediate radiative forcing by black carbon and organic matter with the Specific Forcing Pulse. Atmos. Chem. Phys. 11, 1505–1525. https://doi.org/10.5194/acp-11-1505-2011

Briggs, N.L., Long, C.M., 2016. Critical review of black carbon and elemental carbon source apportionment in Europe and the United States. Atmos. Environ. 144, 409–427. https://doi.org/10.1016/j.atmosenv.2016.09.002

Chameides, W.L., Yu, H., Liu, S.C., Bergin, M., Zhou, X., Mearns, L., Wang, G., Kiang, C.S., Saylor, R.D., Luo, C., Huang, Y., Steiner, A., Giorgi, F., 1999. Case study of the effects of atmospheric aerosols and regional haze on agriculture: An opportunity to enhance crop yields in China through emission controls? Proc. Natl. Acad. Sci. U. S. A. 96, 13626–13633. https://doi.org/10.1073/pnas.96.24.13626

706 Chang, D., Li, Q., Wang, Z., Dai, J., Fu, X., Guo, J., Zhu, L., Pu, D., Cuevas, C.A.,
707 Fernandez, R.P., Wang, W., Ge, M., Fung, J.C.H., Lau, A.K.H., Granier, C., Brasseur,
708 G., Pozzer, A., Saiz-Lopez, A., Song, Y., Wang, T., 2024. Significant chlorine emissions
709 from biomass burning affect the long-term atmospheric chemistry in Asia. Natl. Sci.
710 Rev. 11. https://doi.org/10.1093/nsr/nwae285

711 Chauhan, S., 2010. Biomass resources assessment for power generation: A case study from
712 Haryana state, India. Biomass and Bioenergy 34, 1300–1308.
713 https://doi.org/10.1016/j.biombioe.2010.04.003

714 Chen, B., Andersson, A., Lee, M., Kirillova, E.N., Xiao, Q., Kruså, M., Shi, M., Hu, K., Lu,
715 Z., Streets, D.G., Du, K., Gustafsson, Ö., 2013. Source forensics of black carbon
716 aerosols from China. Environ. Sci. Technol. 47, 9102–9108.
717 https://doi.org/10.1021/es401599r

718 Chen, Y., Schleicher, N., Fricker, M., Cen, K., Liu, X.L., Kaminski, U., Yu, Y., Wu, X.F.,
719 Norra, S., 2016. Long-term variation of black carbon and PM2.5 in Beijing, China with
720 respect to meteorological conditions and governmental measures. Environ. Pollut. 212,
721 269–278. https://doi.org/10.1016/j.envpol.2016.01.008

722 Dumka, U.C., Kaskaoutis, D.G., Devara, P.C.S., Kumar, R., Kumar, S., Tiwari, S.,
723 Gerasopoulos, E., Mihalopoulos, N., 2019. Year-long variability of the fossil fuel and
724 wood burning black carbon components at a rural site in southern Delhi outskirts.
725 Atmos. Res. 216, 11–25. https://doi.org/10.1016/j.atmosres.2018.09.016

726 Dumka, U.C., Kaskaoutis, D.G., Tiwari, S., Safai, P.D., Attri, S.D., Soni, V.K., Singh, N.,
727 Mihalopoulos, N., 2018. Assessment of biomass burning and fossil fuel contribution to
728 black carbon concentrations in Delhi during winter. Atmos. Environ. 194, 93–109.
729 https://doi.org/10.1016/j.atmosenv.2018.09.033

730 Epa, U.S., 2013. Environmental Technology Verification Report Cooper Environmental
731 Services LLC †.

732 Faisal, M., Ali, U., Kumar, A., Hazarika, N., Singh, V., Kumar, M., 2024. Festive fireworks
733 in Delhi: A major source of elemental aerosols established through dispersion
734 normalized PMF in a multiyear study. Atmos. Environ. 323, 120394.
735 https://doi.org/10.1016/j.atmosenv.2024.120394

736 Faisal, M., Ali, U., Kumar, A., Kumar, M., Singh, V., 2025. Unveiling PM2.5 sources:
737 Double and tracer conjugate PMF approaches for high-resolution organic, BC, and
738 inorganic PM2.5 data. Atmos. Environ. 343, 121011.
739 https://doi.org/10.1016/j.atmosenv.2024.121011

740 Favez, O., El Haddad, I., Piot, C., Boréave, A., Abidi, E., Marchand, N., Jaffrezo, J.L.,
741 Besombes, J.L., Personnaz, M.B., Sciare, J., Wortham, H., George, C., D'Anna, B.,
742 2010. Inter-comparison of source apportionment models for the estimation of wood
743 burning aerosols during wintertime in an Alpine city (Grenoble, France). Atmos. Chem.
744 Phys. 10, 5295–5314. https://doi.org/10.5194/acp-10-5295-2010

745 Fitch, J., 2019. Copper and your Diesel engine.

746 Freitas, S.R., Grell, G.A., Li, H., 2021. The Grell-Freitas (GF) convection parameterization:
747 Recent developments, extensions, and applications. Geosci. Model Dev. 14, 5393–5411.
748 https://doi.org/10.5194/gmd-14-5393-2021

749 Furger, M., Minguillón, M.C., Yadav, V., Slowik, J.G., Hüglin, C., Fröhlich, R., Petterson,
750 K., Baltensperger, U., Prévôt, A.S.H., 2017. Elemental composition of ambient aerosols
751 measured with high temporal resolution using an online XRF spectrometer. Atmos.
752 Meas. Tech. 10, 2061–2076. https://doi.org/10.5194/amt-10-2061-2017

753 Ganguly, D., Jayaraman, A., Rajesh, T.A., Gadhavi, H., 2006. Wintertime aerosol properties

754 during foggy and nonfoggy days over urban center Delhi and their implications for
755 shortwave radiative forcing. J. Geophys. Res. Atmos. 111.
756 https://doi.org/10.1029/2005JD007029

757 Goel, V., Mishra, S.K., Pal, P., Ahlawat, A., Vijayan, N., Jain, S., Sharma, C., 2020.
758 Influence of Chemical Aging on Physico-chemical Properties of Mineral Dust Particles:
759 A Case Study of 2016 Dust Storms over Delhi. Environmental Pollution 115338.
760 https://doi.org/10.1016/j.envpol.2020.115338

761 Goel, V., Hazarika, N., Kumar, M., Singh, V., 2021a. Source apportionment of black carbon
762 over Delhi: A case study of extreme biomass burning events and Diwali festival. Urban
763 Clim. 39, 100926. https://doi.org/10.1016/j.uclim.2021.100926

764 Goel, V., Hazarika, N., Kumar, M., Singh, V., Thamban, N.M., Tripathi, S.N., 2021b.
765 Variations in Black Carbon concentration and sources during COVID-19 lockdown in
766 Delhi. Chemosphere 270, 129435. https://doi.org/10.1016/j.chemosphere.2020.129435

767 Goel, V., Jain, S., Singh, V., Kumar, M., 2023a. Source apportionment, health risk
768 assessment, and trajectory analysis of black carbon and light absorption properties of
769 black and brown carbon in Delhi, India. Environ. Sci. Pollut. Res. Int. 30, 116252–
770 116265. https://doi.org/10.1007/s11356-023-30512-w

771 Goel, V., Kumar, A., Jain, S., Singh, V., Kumar, M., 2023b. Spatiotemporal variability and
772 health risk assessment of PM2.5 and NO2 over the Indo-Gangetic Plain: A three years
773 long study (2019-21). Environ. Monit. Assess. 195, 1–17.
774 https://doi.org/10.1007/s10661-023-11558-2

775 Gong, X., Zhang, C., Chen, H., Nizkorodov, S.A., Chen, J., Yang, X., 2016. Size distribution
776 and mixing state of black carbon particles during a heavy air pollution episode in
777 Shanghai. Atmos. Chem. Phys. 16, 5399–5411. https://doi.org/10.5194/acp-16-5399-

2016

Grigoratos, T., Martini, G., 2015. Brake wear particle emissions: a review. Environ. Sci. Pollut. Res. 22, 2491–2504. https://doi.org/10.1007/s11356-014-3696-8

Gupta, P., Singh, S.P., Jangid, A., Kumar, R., 2017. Characterization of black carbon in the ambient air of Agra, India: Seasonal variation and meteorological influence. Adv. Atmos. Sci. 34, 1082–1094. https://doi.org/10.1007/s00376-017-6234-z

Gustafsson, Ö., Kruså, M., Zencak, Z., Sheesley, R.J., Granat, L., Engström, E., Praveen, P.S., Rao, P.S.P., Leck, C., Rodhe, H., 2009. Brown clouds over South Asia: Biomass or fossil fuel combustion? Science (80-.). 323, 495–498. https://doi.org/10.1126/science.1164857

Herich, H., Hueglin, C., Buchmann, B., 2011. A 2.5 year's source apportionment study of black carbon from wood burning and fossil fuel combustion at urban and rural sites in Switzerland. Atmos. Meas. Tech. 4, 1409–1420. https://doi.org/10.5194/amt-4-1409-2011

Intergovernmental Panel on Climate Change (IPCC), 2023. Climate Change 2021 – The Physical Science Basis. Clim. Chang. 2021 – Phys. Sci. Basis. https://doi.org/10.1017/9781009157896

Jacob, D.J., Winner, D.A., 2009. Effect of climate change on air quality. Atmos. Environ. 43, 51–63. https://doi.org/10.1016/j.atmosenv.2008.09.051

Janssen, N.A.H., Hoek, G., Simic-Lawson, M., Fischer, P., van Bree, L., Brink, H. Ten, Keuken, M., Atkinson, R.W., Ross Anderson, H., Brunekreef, B., Cassee, F.R., 2011. Black carbon as an additional indicator of the adverse health effects of airborne particles compared with pm10 and pm2.5. Environ. Health Perspect. 119, 1691–1699. https://doi.org/10.1289/ehp.1003369

802 Jiang, K., Xing, R., Luo, Z., Huang, W., Yi, F., Men, Y., Zhao, N., Chang, Z., Zhao, J., Pan,
803 B., Shen, G., 2024. Pollutant emissions from biomass burning: A review on emission
804 characteristics, environmental impacts, and research perspectives. Particuology 85, 296–
805 309. https://doi.org/10.1016/j.partic.2023.07.012

806 Khare, P., Baruah, B.P., Rao, P.G., 2011. Water-soluble organic compounds (WSOCs) in
807 PM2.5 and PM10 at a subtropical site of India. Tellus, Ser. B Chem. Phys. Meteorol. 63,
808 990–1000. https://doi.org/10.1111/j.1600-0889.2011.00564.x

809 Kim, K.H., Kabir, E., Kabir, S., 2015. A review on the human health impact of airborne
810 particulate matter. Environ. Int. 74, 136–143.
811 https://doi.org/10.1016/j.envint.2014.10.005

812 Kirchstetter, T.W., Novakov, T., Hobbs, P. V., 2004. Evidence that the spectral dependence
813 of light absorption by aerosols is affected by organic carbon. J. Geophys. Res. D Atmos.
814 109, 1–12. https://doi.org/10.1029/2004JD004999

815 Kumar, A., Goel, V., Faisal, M., Ali, U., Maity, R., Ganguly, D., Singh, V., Kumar, M.,
816 2024. Two different approaches for source apportionment of ambient black carbon in
817 highly polluted environments. Atmos. Environ. 338, 120863.
818 https://doi.org/10.1016/j.atmosenv.2024.120863

819 Li, J., Pósfai, M., Hobbs, P. V., Buseck, P.R., 2003. Individual aerosol particles from biomass
820 burning in southern Africa: 2. Compositions and aging of inorganic particles. J.
821 Geophys. Res. Atmos. 108, 1–12. https://doi.org/10.1029/2002jd002310

822 Manchanda, C., Kumar, M., Singh, V., Faisal, M., Hazarika, N., Shukla, A., Lalchandani, V.,
823 Goel, V., Thamban, N., Ganguly, D., Tripathi, S.N., 2021. Variation in chemical
824 composition and sources of PM2.5 during the COVID-19 lockdown in Delhi. Environ.
825 Int. 153, 106541. https://doi.org/10.1016/j.envint.2021.106541

826 Kumar, M. (2011). *Multiscale CFD simulations of entrained flow gasification* (Doctoral
827 dissertation, Massachusetts Institute of Technology).

828 Ministry of Power directives, R.I. 1945245, 2023. Revised Biomass Policy mandates 5%
829 biomass co-firing in Thermal Power Plants from FY 2024-2025.

830 Monaghan, R. F., Kumar, M., Singer, S. L., Zhang, C., & Ghoniem, A. F. (2009, January).
831 Reduced order modeling of entrained flow solid fuel gasification. In ASME
832 International Mechanical Engineering Congress and Exposition (Vol. 43765, pp. 397-
833 409).Mousavi, A., Sowlat, M.H., Hasheminassab, S., Polidori, A., Sioutas, C., 2018.
834 Spatio-temporal trends and source apportionment of fossil fuel and biomass burning
835 black carbon (BC) in the Los Angeles Basin. Sci. Total Environ. 640–641, 1231–1240.
836 https://doi.org/10.1016/j.scitotenv.2018.06.022

837 Obernberger, I., Brunner, T., Bärnthaler, G., 2006. Chemical properties of solid biofuels-
838 significance and impact. Biomass and Bioenergy 30, 973–982.
839 https://doi.org/10.1016/j.biombioe.2006.06.011

840 Paatero, P., 1999. The Multilinear Engine—A Table-Driven, Least Squares Program for
841 Solving Multilinear Problems, Including the n-Way Parallel Factor Analysis Model. J.
842 Comput. Graph. Stat. 8, 854–888. https://doi.org/10.1080/10618600.1999.10474853

843 Paatero, P., Tapper, U., 1994. Positive matrix factorization: A non-negative factor model with
844 optimal utilization of error estimates of data values. Environmetrics 5, 111–126.
845 https://doi.org/10.1002/env.3170050203

846 Pant, P., Harrison, R.M., 2012. Critical review of receptor modelling for particulate matter: A
847 case study of India. Atmos. Environ. https://doi.org/10.1016/j.atmosenv.2011.11.060

848 Petit, J.-E., Favez, O., Sciare, J., Canonaco, F., Croteau, P., Močnik, G., Jayne, J., Worsnop,
849 D., Leoz-Garziandia, E., 2014. Submicron aerosol source apportionment of wintertime

pollution in Paris, France by double positive matrix factorization (PMF²) using an aerosol chemical speciation monitor (ACSM) and a multi-wavelength Aethalometer. Atmos. Chem. Phys. 14, 13773–13787. https://doi.org/10.5194/acp-14-13773-2014

Pósfai, M., Simonics, R., Li, J., Hobbs, P. V., Buseck, P.R., 2003. Individual aerosol particles from biomass burning in southern Africa: 1. Compositions and size distributions of carbonaceous particles. J. Geophys. Res. Atmos. 108, 1–13. https://doi.org/10.1029/2002jd002291

Rai, P., Furger, M., El Haddad, I., Kumar, V., Wang, L., Singh, A., Dixit, K., Bhattu, D., Petit, J.E., Ganguly, D., Rastogi, N., Baltensperger, U., Tripathi, S.N., Slowik, J.G., Prévôt, A.S.H., 2020. Real-time measurement and source apportionment of elements in Delhi's atmosphere. Sci. Total Environ. 742, 140332. https://doi.org/10.1016/j.scitotenv.2020.140332

Reche, C., Rivas, I., Pandolfi, M., Viana, M., Bouso, L., Àlvarez-Pedrerol, M., Alastuey, A., Sunyer, J., Querol, X., 2015. Real-time indoor and outdoor measurements of black carbon at primary schools. Atmos. Environ. 120, 417–426. https://doi.org/10.1016/j.atmosenv.2015.08.044

Reddington, C.L., McMeeking, G., Mann, G.W., Coe, H., Frontoso, M.G., Liu, D., Flynn, M., Spracklen, D. V., Carslaw, K.S., 2013. The mass and number size distributions of black carbon aerosol over Europe. Atmos. Chem. Phys. 13, 4917–4939. https://doi.org/10.5194/acp-13-4917-2013

Reddy, M.S., Venkataraman, C., 2002. Inventory of aerosol and sulphur dioxide emissions from India: I - Fossil fuel combustion. Atmos. Environ. 36, 677–697. https://doi.org/10.1016/S1352-2310(01)00463-0

874 Sandradewi, J., Prévôt, a. S.H., Alfarra, M.R., Szidat, S., Wehrli, M.N., Ruff, M., Weimer,
875 S., Lanz, V. a., Weingartner, E., Perron, N., Caseiro, a., Kasper-Giebl, a., Puxbaum, H.,
876 Wacker, L., Baltensperger, U., 2008. Comparison of several wood smoke markers and
877 source apportionment methods for wood burning particulate mass. Atmos. Chem. Phys.
878 Discuss. 8, 8091–8118.

879 Schmid, O., Artaxo, P., Arnott, W.P., Chand, D., Gatti, L. V., Frank, G.P., Hoffer, A.,
880 Schnaiter, M., Andreae, M.O., 2006. Spectral light absorption by ambient aerosols
881 influenced by biomass burning in the Amazon Basin. I: Comparison and field calibration
882 of absorption measurement techniques. Atmos. Chem. Phys. 6, 3443–3462.
883 https://doi.org/10.5194/acp-6-3443-2006

884 Sharma, S.K., Mandal, T.K., Jain, S., Saraswati, Sharma, A., Saxena, M., 2016. Source
885 Apportionment of PM2.5 in Delhi, India Using PMF Model. Bull. Environ. Contam.
886 Toxicol. 97, 286–293. https://doi.org/10.1007/s00128-016-1836-1

887 Shukla, A.K., Lalchandani, V., Bhattu, D., Dave, J.S., Rai, P., Thamban, N.M., Mishra, S.,
888 Gaddamidi, S., Tripathi, N., Vats, P., Rastogi, N., Sahu, L., Ganguly, D., Kumar, M.,
889 Singh, V., Gargava, P., Tripathi, S.N., 2021. Real-time quantification and source
890 apportionment of fine particulate matter including organics and elements in Delhi during
891 summertime. Atmos. Environ. 261. https://doi.org/10.1016/j.atmosenv.2021.118598

892 Shukla, A. K., Tripathi, S. N., Canonaco, F., Lalchandani, V., Sahu, R., Srivastava, D., ... &
893 Rastogi, N. (2023). Spatio-temporal variation of C-PM2. 5 (composition based PM2. 5)
894 sources using PMF* PMF (double-PMF) and single-combined PMF technique on real-
895 time non-refractory, BC and elemental measurements during post-monsoon and winter
896 at two sites in Delhi, India. *Atmospheric Environment*, *293*, 119456.

897 Soltes, E.J., Elder, T.J., 1981. Pyrolysis. In organic chemicals from biomass, Goldstein, I. S.,

898 Ed.; CRC Press: Boca Raton, FL.

899 Thorpe, A., Harrison, R.M., 2008. Sources and properties of non-exhaust particulate matter
900 from road traffic: A review. Sci. Total Environ. 400, 270–282.
901 https://doi.org/10.1016/j.scitotenv.2008.06.007

902 Tiwari, S., Pipal, A.S., Srivastava, A.K., Bisht, D.S., Pandithurai, G., 2015. Determination of
903 wood burning and fossil fuel contribution of black carbon at Delhi, India using aerosol
904 light absorption technique. Environ. Sci. Pollut. Res. 22, 2846–2855.
905 https://doi.org/10.1007/s11356-014-3531-2

906 Tiwari, S., Srivastava, A.K., Bisht, D.S., Safai, P.D., Parmita, P., 2013. Assessment of
907 carbonaceous aerosol over Delhi in the Indo-Gangetic Basin: Characterization, sources
908 and temporal variability. Nat. Hazards 65, 1745–1764. https://doi.org/10.1007/s11069-
909 012-0449-1

910 Ulbrich, I.M., Canagaratna, M.R., Zhang, Q., Worsnop, D.R., Jimenez, J.L., 2009.
911 Interpretation of organic components from Positive Matrix Factorization of aerosol mass
912 spectrometric data. Atmos. Chem. Phys. 9, 2891–2918. https://doi.org/10.5194/acp-9-
913 2891-2009

914 Vaishya, A., Singh, P., Rastogi, S., Babu, S.S., 2017. Aerosol black carbon quantification in
915 the central Indo-Gangetic Plain: Seasonal heterogeneity and source apportionment.
916 Atmos. Res. 185, 13–21. https://doi.org/10.1016/j.atmosres.2016.10.001

917 Viana, M., Kuhlbusch, T.A.J., Querol, X., Alastuey, A., Harrison, R.M., Hopke, P.K.,
918 Winiwarter, W., Vallius, M., Szidat, S., Prévôt, A.S.H., Hueglin, C., Bloemen, H.,
919 Wåhlin, P., Vecchi, R., Miranda, A.I., Kasper-Giebl, A., Maenhaut, W., Hitzenberger,
920 R., 2008. Source apportionment of particulate matter in Europe: A review of methods
921 and results. J. Aerosol Sci. 39, 827–849. https://doi.org/10.1016/j.jaerosci.2008.05.007

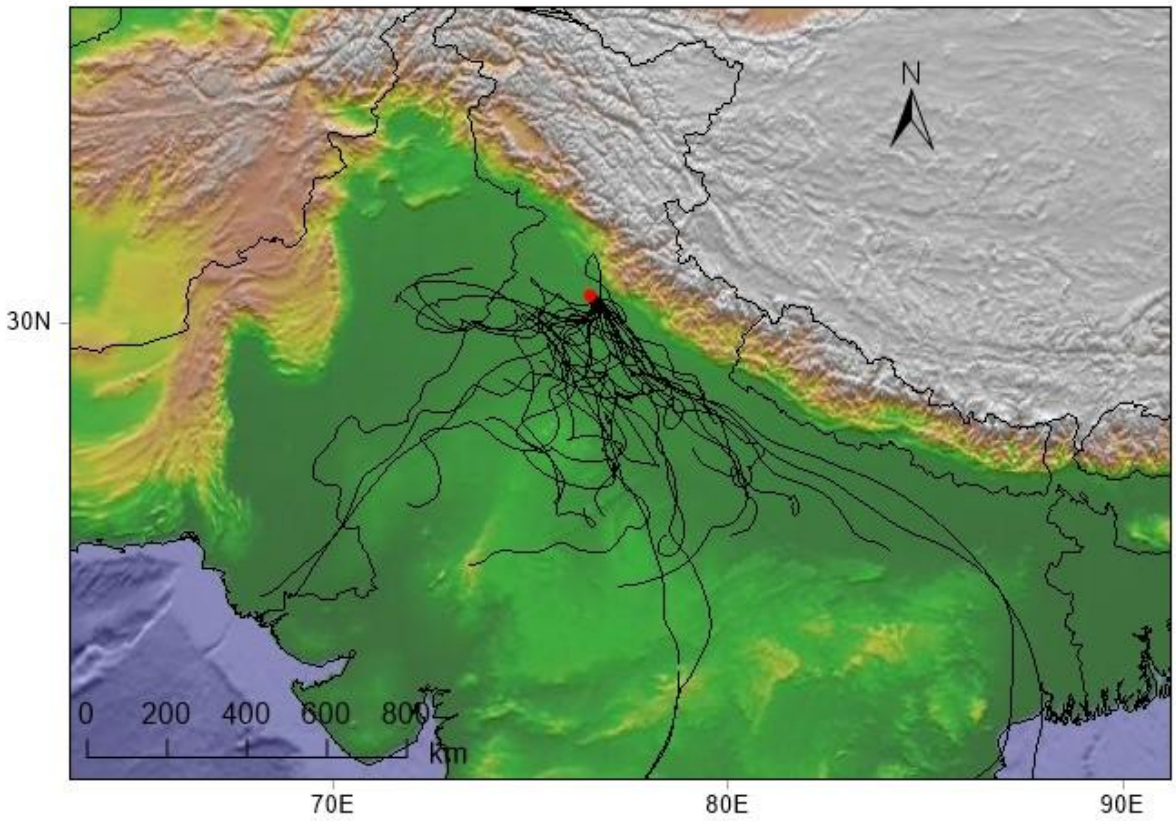
Vossler, T., Černikovský, L., Novák, J., Williams, R., 2016. Source apportionment with uncertainty estimates of fine particulate matter in Ostrava, Czech Republic using Positive Matrix Factorization. Atmos. Pollut. Res. 7, 503–512. https://doi.org/10.1016/j.apr.2015.12.004

Yang, J., Kang, S., Ji, Z., Chen, D., 2018. Modeling the Origin of Anthropogenic Black Carbon and Its Climatic Effect Over the Tibetan Plateau and Surrounding Regions. J. Geophys. Res. Atmos. 123, 671–692. https://doi.org/10.1002/2017JD027282

Zhang, X., Chen, X., Wang, J., 2019. A number-based inventory of size-resolved black carbon particle emissions by global civil aviation. Nat. Commun. 10, 1–11. https://doi.org/10.1038/s41467-019-08491-9

944

945



946

Figure 1: The forward wind trajectories illustrate the transport pathways moving from sampling site, Punjab toward the Indo-Gangetic Plain (IGP) region.

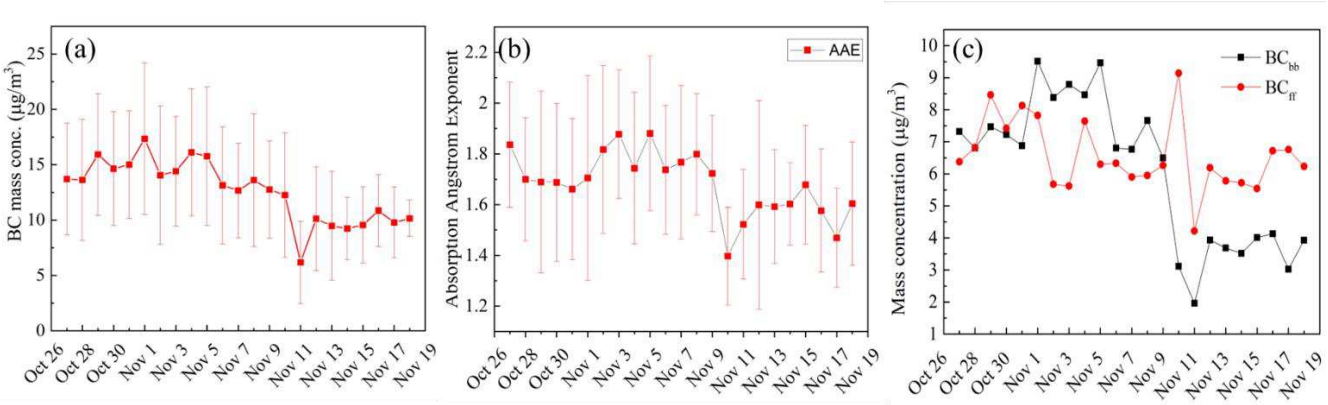


Figure 2: Temporal variations of BC (a), AAE (b) and BC_{bb}, and BC_{ff} from the Aethalometer model (c).

947

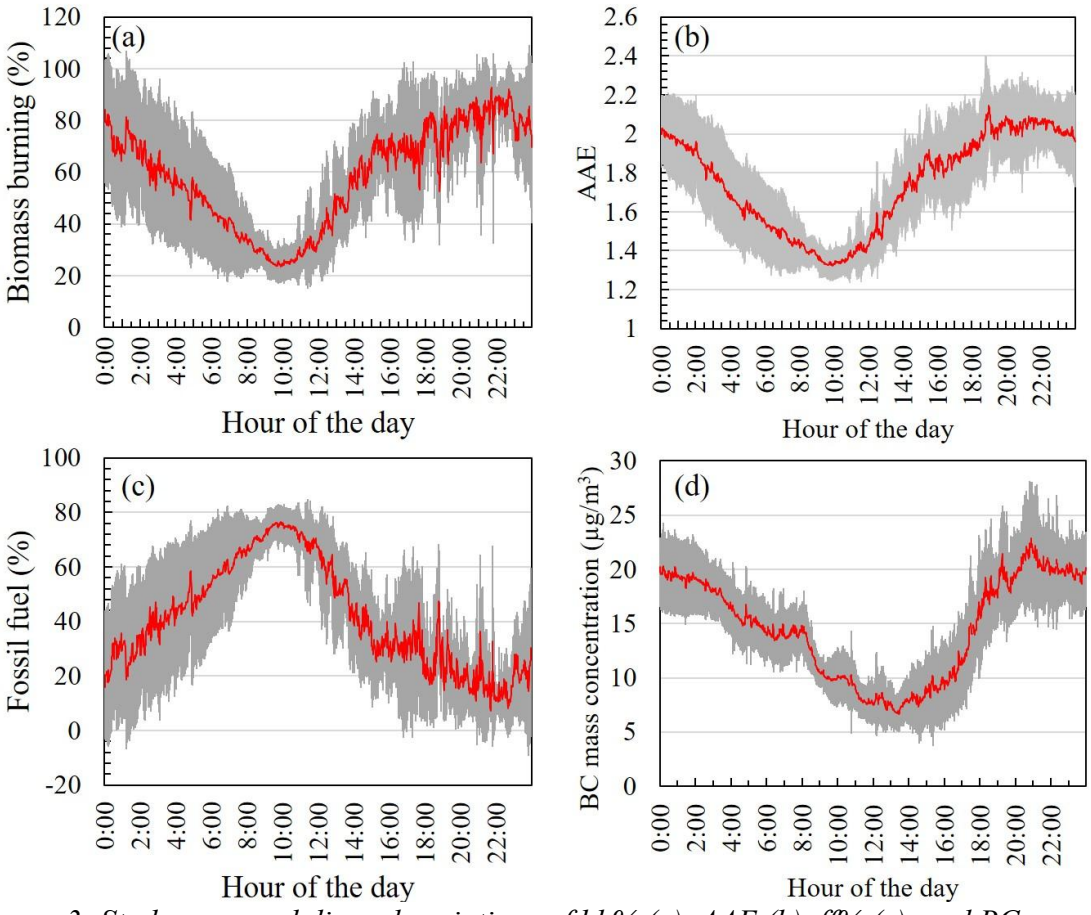


Figure 3: Study averaged diurnal variations of bb% (a), AAE (b), ff% (c), and BC mass concentration (d).

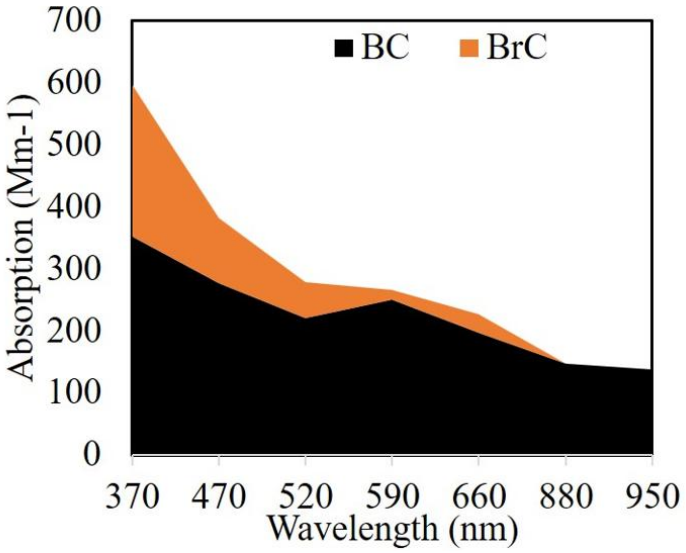


Figure 4: Spectral variation of absorption coefficients of BC and BrC.

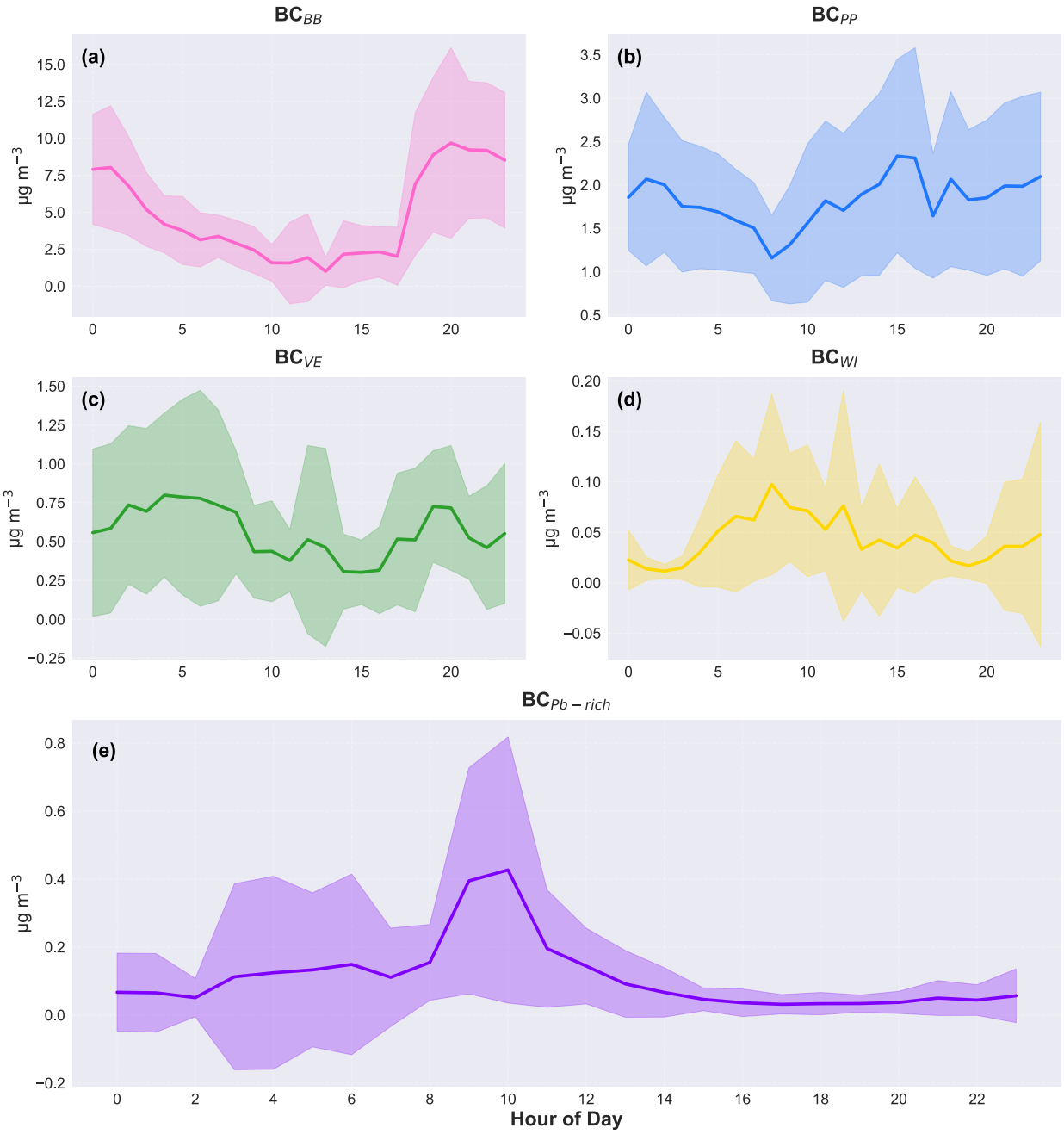


Figure 5: Diurnal variation of BC factors obtained from the PMF model.

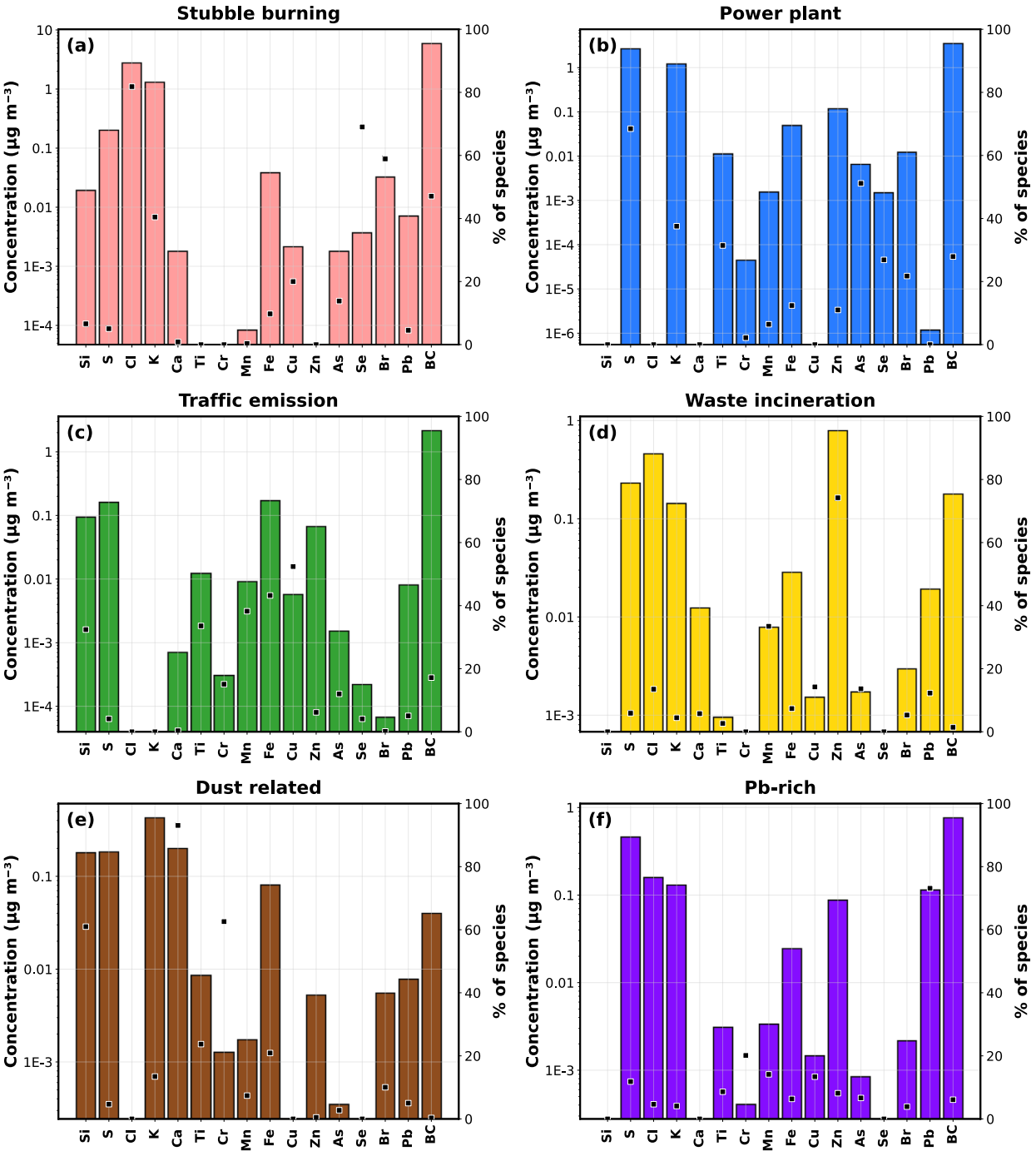


Figure 6: Source profiles of the BC factors identified through PMF model. The bars represent the concentration of each species within a factor plotted on a logarithmic scale, while the square dots indicate the percentage contribution of each species across the factors.

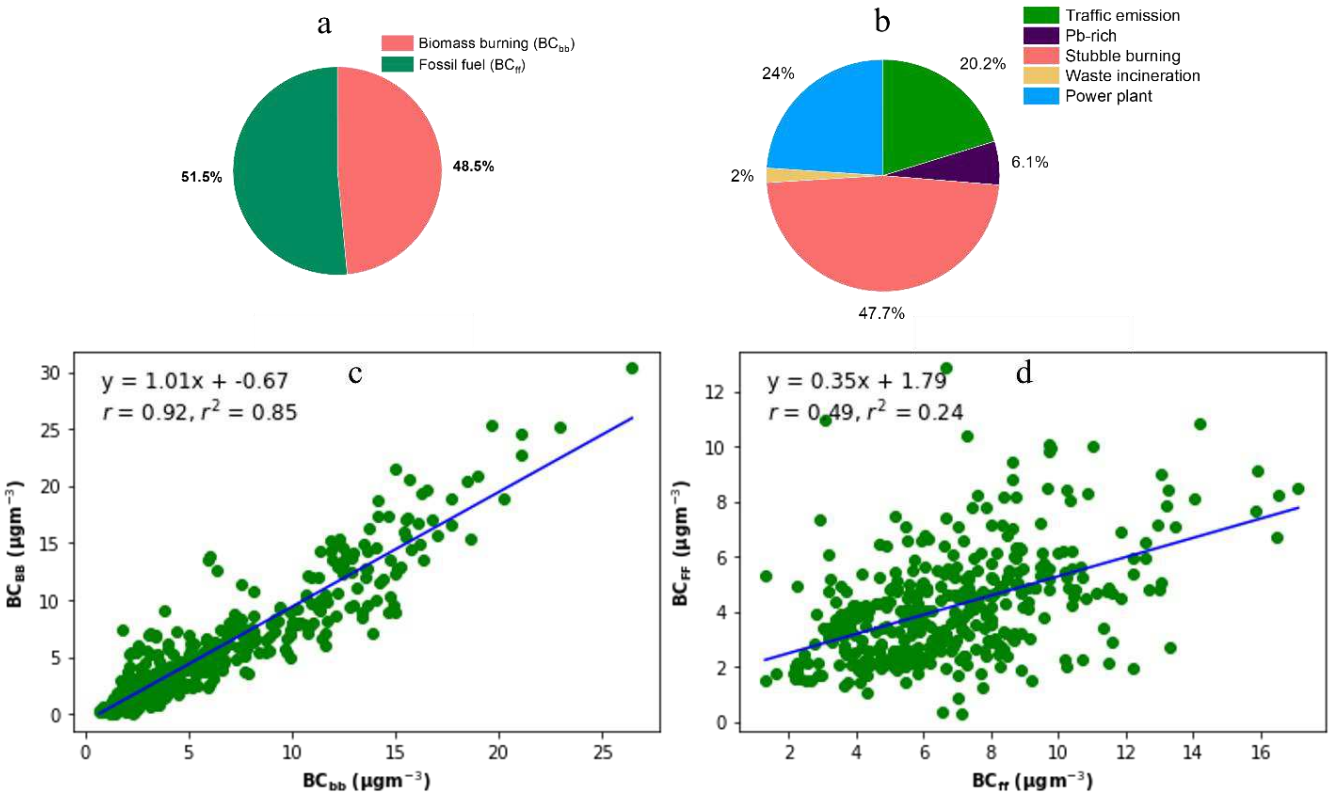


Figure 7: Source contributions to black carbon (BC) estimated using (a) the Aethalometer model and (b) the PMF model. Scatter plot of biomass burning factor (a) and fossil fuel (b) obtained from the aethalometer model and PMF model

982

983

Supplementary Files

This is a list of supplementary files associated with this preprint. Click to download.

- ListoftablesEMS.docx
- SupplementaryEMSPunjab.docx